

# Noise-induced topological transformations of vortex solitons in optical fibers filled with a cold atomic gas

A.V. Prokhorov,<sup>1,\*</sup> M.G. Gladush,<sup>2</sup> M.Yu. Gubin,<sup>1</sup> A.Yu. Leksin,<sup>1</sup> and S.M. Arakelian<sup>1</sup>

<sup>1</sup>*Department of Physics and Applied Mathematics,  
Stoletovs Vladimir State University, Gorkiy str. 87, Vladimir, 600000, Russia*

<sup>2</sup>*Institute for Spectroscopy of the Russian Academy of Sciences,  
Fizicheskaya Str. 5, Troitsk, Moscow, 142190, Russia*

(Dated: March 26, 2013)

We consider the influence of optical and temperature-dependent atomic fluctuations on the formation and propagation of optical vortex solitons in dense media realized as hollow-core optical fibers filled with a cold atomic gas in presence of optical pumping. We show different perturbation-induced scenarios of complete destruction and smooth transformations of the topological characteristics of localized optical structures in hollow-core fiber. The maximum levels of optical and atomic fluctuations at which the soliton regime can be maintained has been determined. The estimates for these levels show an opportunity to observe the optical vortex solitons in the core-filling gas of the fiber for temperatures smaller than the critical temperature for Bose-Einstein condensate.

## I. INTRODUCTION

The study of the formation and propagation of localized spatial optical structures in different media [1] is one of the important issues of modern applied atom optics. It is associated with a wide range of applications, some of which are the problems of data transmission and processing [2]. The greatest interest here is the special class of optical topological structures known as optical vortices [3]. The dark center for those could be registered reliably in experiments even in the case of a strong diffraction broadening of the optical beams [4]. It is relatively easy to obtain such structures in laser cavities [5] or spatially inhomogeneous media [6]. However, the maintenance of the stability conditions for such structures when they propagate in the real media is a difficult task. The soliton modes of optical vortices have so far been observed quite rarely even within short distances [7]. At the same time the distances required for telecommunications have not been worked through at all. The explanation for this is the fact that a full-scale solution to the problem of developing such information channels requires a correct determination of the stability regions [8] fulfilled in the parameters of a laser experiment as well as the stress tests with perturbations for the propagating localized optical structures.

Formation of the stable optical structures occurs near the lasing threshold [2], where the nonlinear effects are very strong. Therefore the solution of this problem requires a strict account of the higher-order nonlinearities and nonlinear absorption effects which are crucial for stability of the optical structures [2, 9]. In experiments in order to realize an optical control of the parameters when entering the soliton mode it is most beneficial to use the  $\Lambda$ -type interaction configuration in a resonant atomic medium with a probe localized structure and a pump

field. The observations of the strong nonlinear effects in such a scheme can be associated with the realization of the Raman regime [9, 10], when the detunings of the electromagnetic fields from the atomic transitions are much higher than the corresponding decay rates (with account for the optical depth of the medium, see [11]).

Among promising media for observation and control of solitons we can mark out the recently created hollow-core optical fibres filled with a cold atomic gas [12]. First, it would allow us to observe the coherent Raman scattering and study the competition between the nonlinear, diffraction and dissipative effects for the probe pulse over short distances [13, 14]. Second, the use of cold atoms opens new possibilities of precision and efficient control over the optical properties of the system. Indeed, in a cold medium we may neglect the effects of the spectral line broadening and splitting as well as assume the minimum impact from the thermal noise.

Obviously, the quality of transmission and the processing rate in the optical data channel [15] is strongly dependent on the efficiency of nonlinear transformations, which significantly increases with the density of resonant atoms in the medium. However, for media with a large density of optically active particles it is necessary to take into account the effective or the local value of the field acting on them [16–19]. The atom-field interaction becomes trickier in this case and in the literature it is known as the consequence of the near dipole-dipole interactions (NDD). This may significantly modify the picture of the phenomenon as the conventional Rabi frequency for an atomic transition is comparable to the corresponding NDD correction term. The estimations for ensembles of resonant particles show that the NDD or the local field effects may be very significant starting from density  $\rho = 10^{15} \text{ cm}^{-3}$ . In connection to this complication, some special attention should be paid to the problem of obtaining stable dynamics of spatial solitons and optical vortices in particular [3] in dense media with an additional view to the perturbations in the medium and the

---

\* avprokhorov@vlsu.ru

field.

The influence of the noise effects on soliton solutions of the nonlinear Schrödinger equation (NLS) has been well studied in the literature and a violation of dynamic equilibrium in such a system is usually observed for the values of the noise intensity, comparable to the main parameters of the problem [20]. A particularly strong presence of the noise in this problem manifests itself near the zero dispersion point, when the short-term changes of the dispersion sign initiated by fluctuations in the medium would quickly destroy the soliton. Only some original pinning method can help to restore the system's working characteristics [21]. Analysis of the fluctuations influence on the dissipative solitons is usually performed artificially by introducing a noise source to the Ginzburg-Landau equation (GLE) [22, 23]. However, this approach does not answer the question about the nature of the noise, and is therefore not possible to assess the contribution of the various physical components into the overall picture of the development of instabilities in the system. This is especially true in the case of the optical solitons in gaseous media, where the density fluctuations at small scales can be comparable with the average density over the entire medium [24, 25]. Even transition to the Bose-Einstein condensate (BEC) can not solve the problem completely because in such a system there are intricate dependencies of density fluctuations on the trapping geometry and the type of interaction between the particles [26, 27].

In this paper we consider the problem of obtaining a stable spatial dynamics of optical vortices [3] in the dense media of BEC-filled optical fibers in presence of optical pumping. The problem is similar to the observation of temporal self-induced transparency solitons in microstructured materials considering the influence of the local field effects [18]. Secondly, in this paper we study the effect of random and/or periodic perturbation of the system's parameters on the process of stabilization and shape evolution of the vortex solitons propagating in a fiber filled with a cold gas.

## II. GENERALIZED DENSITY MATRIX EQUATIONS FOR $\Lambda$ -TYPE ATOM-FIELD INTERACTION IN A DENSE MEDIUM

In this paper we assume that a probe light pulse of given shape  $\mathbf{E}_p$  with the center frequency  $\omega_p$  propagates along axis  $z$  of a hollow-core optical fiber filled with a gas of cold atoms with a temperature  $T$  near the critical temperature [28] of the phase transition:

$$T_{cr} = \frac{\hbar\omega_0}{k_B} \left( \frac{N}{\zeta(3)} \right)^{1/3},$$

where  $\hbar$  is the Planck constant,  $k_B$  is the Boltzmann constant,  $N$  is the total number of particles,  $\omega_0$  is the trapping frequency, and  $\zeta(3)$  is the zeta function of Riemann. It propagates in the direction opposite to cw pump radiation  $\mathbf{E}_c$  as illustrated in Fig. 1a. It propagates in the direction opposite to cw pump radiation  $\mathbf{E}_c$  as illustrated in Fig. 1a. In the Raman limit the probe field detuning  $\Delta_b$  should be substantially greater than the relaxation rate of  $\Gamma_{ab}$  ( $\Gamma_{ac}$ ) from the excited state  $|a\rangle$  (see Fig. 1b). As applied to this problem, the parameter of optical depth of the medium  $d_0$  can be determined through the characteristic linear dimension  $a_0$  of topological structures formed in the  $xOy$  plane as  $d_0 = g^2 N a_0 / (c \Gamma_{ac})$  (compare with [10]). Here  $g = \mu_{ba} \sqrt{\omega / 2 \hbar \varepsilon_0 V}$  is the atom-field coupling constant,  $\varepsilon = A_p \sqrt{2 \varepsilon_0 V / \hbar \omega}$ ,  $A_p$  is slowly varying amplitude of the probe field,  $V$  is the quantization volume,  $N = \rho V_0$  is the number of atoms in the interaction zone of volume  $V_0$  for atomic density  $\rho$ ,  $c$  is the speed of light in vacuum,  $\varepsilon_0$  is the vacuum permittivity. The frequency separation between levels  $|b\rangle$  and  $|c\rangle$  is  $\delta = 6.834 \times 10^9 \text{ s}^{-1}$ , the dipole transition matrix element for  $|b\rangle \rightarrow |a\rangle$  is  $\mu_{ba} = 3.58 \times 10^{-29} \text{ C}\cdot\text{m}$ .

Since  $^{87}\text{Rb}$  atoms have large dipole moments of the desired transitions and taking into account their density inside the hollow core of the fiber the value of NDD interaction  $\chi_{ba} = \rho |\mu_{ba}|^2 / (3 \hbar \varepsilon_0)$  which determines the effective Rabi frequency  $\Omega_{eff} = \Omega_{ba} + \chi_{ba} \sigma_{ba}$  [18] can be close to the value of the Rabi frequency of the probe field (here  $\sigma_{ba}$  is the corresponding of the density matrix element). Thus, the nonlinear optical effects arising in such a system will be determined, on one hand, by the pump field parameters, and on the other hand, by the number density of the atoms hosted by the hollow fiber.

This system is described by the following system of equation for the density matrix elements:

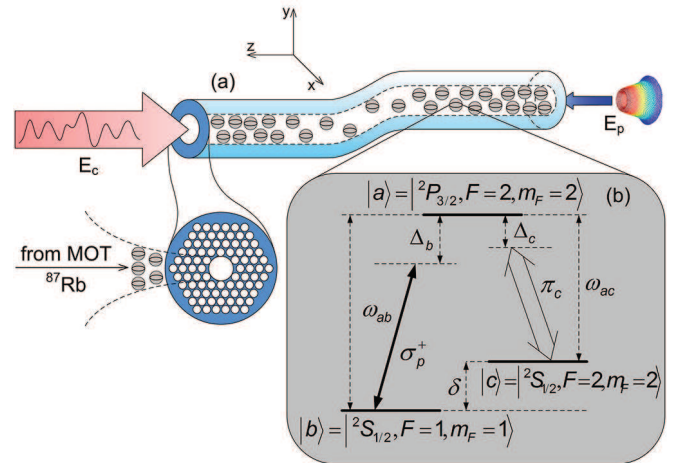


Figure 1. (a) Model diagram of a hollow-core optical fiber filled with an atomic gas (b)  $\Lambda$ -type interaction configuration applied for  $^{87}\text{Rb}$  atoms, energy level splitting between  $|c\rangle$  and  $|b\rangle$  is  $\delta = 6.834 \times 10^9 \text{ s}^{-1}$ , the dipole transition matrix element for  $|a\rangle \rightarrow |b\rangle$  at wavelength  $\lambda = 780.241 \text{ nm}$  is  $\mu_{ab} = 3.58 \times 10^{-29} \text{ C}\cdot\text{m}$ .

$$\begin{aligned}
\dot{\sigma}_{ba} &= i(\Delta_b - \chi_{ba}(\sigma_{bb} - \sigma_{aa}))\sigma_{ba} - ig\varepsilon(\sigma_{bb} - \sigma_{aa}) - i(\Omega + \chi_{ca}\sigma_{ca})\sigma_{bc} - \frac{1}{2}(\Gamma_{ab} + \Gamma_{ac})\sigma_{ba}, \\
\dot{\sigma}_{ca} &= i(\Delta_c - \chi_{ca}(\sigma_{cc} - \sigma_{aa}))\sigma_{ca} - i\Omega(\sigma_{cc} - \sigma_{aa}) - i(g\varepsilon + \chi_{ba}\sigma_{ba})\sigma_{cb} - \frac{1}{2}(\Gamma_{ab} + \Gamma_{ac})\sigma_{ca}, \\
\dot{\sigma}_{bc} &= i(\Delta_b - \Delta_c)\sigma_{bc} + ig\varepsilon\sigma_{ac} - i\Omega^*\sigma_{ba} + i\chi_{ba}\sigma_{ba}\sigma_{ac} - i\chi_{ac}\sigma_{ac}\sigma_{ba}, \\
\dot{\sigma}_{aa} &= ig\varepsilon^*\sigma_{ba} + i\Omega^*\sigma_{ca} - ig\varepsilon\sigma_{ab} - i\Omega^*\sigma_{ac} - (\Gamma_{ab} + \Gamma_{ac})\sigma_{aa}, \\
\dot{\sigma}_{bb} &= ig\varepsilon\sigma_{ab} - ig\varepsilon^*\sigma_{ba} + \Gamma_{ab}\sigma_{aa}, \\
\dot{\sigma}_{cc} &= i\Omega\sigma_{ac} - i\Omega^*\sigma_{ca} + \Gamma_{ac}\sigma_{aa},
\end{aligned} \tag{1}$$

where  $\Omega \equiv \Omega_{ca}$  and  $g\varepsilon \equiv \Omega_{ba}$  are the Rabi frequencies for the pump field and the probe pulse respectively,  $\Delta_b$  and  $\Delta_c$  are the corresponding detunings.

In this section, we consider the applicability of approximations used in the paper for a three-level atomic medium as a result of the different modes of its interaction with the external optical fields. One of the specific requirements to such a problem in our case is the presence of a significant polarization of the medium produced by the contiguous transitions  $|a\rangle \rightarrow |b\rangle$  and  $|a\rangle \rightarrow |c\rangle$ . It is necessary to provide nonlinear control over the probe vortices via the pump wave. Besides, we have to make a set of assumptions that will significantly simplify Eqs. (1) for further analysis. The key point here is to choose the right balance between the Rabi frequency of the pump field, its detuning from the resonance and the decay rate of the excited state.

In general, the propagation equation for a probe field in a resonant medium, taking diffraction into account, is

$$\left( \frac{\partial}{\partial t} + c \frac{\partial}{\partial z} - ic \frac{D}{2} \nabla_{\perp}^2 \right) \varepsilon = -igN\sigma_{ba}, \tag{2}$$

where  $\nabla_{\perp}^2 = \partial^2/\partial x^2 + \partial^2/\partial y^2$ ,  $D = \lambda/\pi$  the diffraction parameter in the plane transverse to axis  $z$ .

Self-consistent solutions of Eqs. (1)-(2) can be found if we use the following approximations. First, we assume that all atoms are initially at level  $b$ , i.e.,  $\sigma_{bb} = 1$ ,  $\sigma_{aa} = \sigma_{cc} = 0$  and the population of the excited state remains small throughout the interaction time, i.e.,  $\sigma_{bb} \cong 1$ ,  $\sigma_{aa(cc)} \cong 0$  (while  $\dot{\sigma}_{ii} \cong 0$  where  $i = a, b, c$ ). Secondly, we believe that when  $\chi_{ca} = \chi_{ba} = \chi$  the contribution of the local field is comparable to the probe Rabi frequency, but it can be omitted for the pump transition, i.e.,  $g\varepsilon \geq \sigma_{ba}\chi_{ba}$  and  $\Omega \gg \sigma_{ca}\chi_{ca}$ . As a result, the final system of equations reduces to the following (simplified) form:

$$\dot{\sigma}_{ba} = -\Gamma_1\sigma_{ba} - ig\varepsilon - i\Omega\sigma_{bc} - i\chi_{ba}\sigma_{ba}, \tag{3a}$$

$$\dot{\sigma}_{ca} = -\Gamma_2\sigma_{ca} - ig\varepsilon\sigma_{cb} - i\chi_{ba}\sigma_{ba}\sigma_{cb}, \tag{3b}$$

$$\dot{\sigma}_{bc} = i\Delta_3\sigma_{bc} + ig\varepsilon\sigma_{ac} - i\Omega^*\sigma_{ba}, \tag{3c}$$

$$\dot{\sigma}_{bb} = ig\varepsilon\sigma_{ab} - ig\varepsilon^*\sigma_{ba}, \tag{3d}$$

where  $\Gamma_1 = -i\Delta_b + 1/2(\Gamma_{ab} + \Gamma_{ac})$ ,  $\Gamma_2 = -i\Delta_c + 1/2(\Gamma_{ab} + \Gamma_{ac})$  and  $\Delta_3 = \Delta_b - \Delta_c$ . In Eqs. (3) the contribution of the local field is presented in two ways. In (3a) its action is trivial and produces an effective frequency shift,

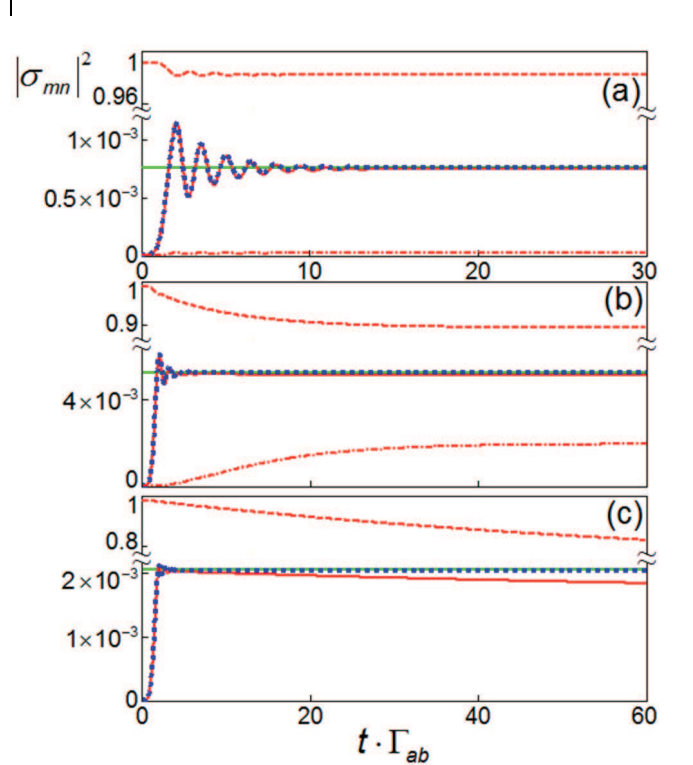


Figure 2. Time dependence of the density matrix elements in units of the excited state lifetime  $\Gamma_{ab}^{-1}$  (a) for the near-resonant (b) Raman modes of  $\Lambda$ -type interaction in the limit of strong coupling, (c) for the near-resonant mode in the limit of weak coupling. The solid line is for  $|\sigma_{ba}|^2$ , dashed is for  $|\sigma_{bb}|^2$  and the dash-dot line is for  $|\sigma_{cc}|^2$ , the red lines are solutions of (1), the dotted blue line is for  $|\sigma_{ba}|^2$  obtained from Eqs. (3). The thick solid green line corresponds to  $|\sigma_{ba}|^2$  which is calculated for the approximate steady-state solution (8).

but in (3b) it provides a significant effect, which is the appearance of the nonlinear coupling between the atomic excitations (polarizations) in the probe  $\sigma_{ba}$  and magnetic  $\sigma_{cb}$  transitions.

Figure 2 shows, in particular, the comparison of the independent solutions of the exact system (1) and the approximate (3) for different modes of the atom-field interactions at probe field switching time of  $\tau_{sw} = 2 \times 10^{-10}$  s and cw pump field. The atomic and field parameters were chosen as follows: the characteristic size of the optical beam  $a_0 = 20 \mu\text{m}$ , the atomic density  $\rho = 1.01 \times 10^{22} \text{m}^{-3}$ , the relaxation rate  $\Gamma_{ab} = \Gamma_{ac} = 10^9 \text{s}^{-1}$ , the probe

field intensity  $I_p = 0.22 \text{ W}\cdot\text{cm}^{-2}$ , the pump intensity  $I_c = 146.5 \text{ W}\cdot\text{cm}^{-2}$ , the probe detuning  $\Delta_b = -5 \times 10^9 \text{ s}^{-1}$ . The corresponding Rabi frequencies can be calculated as  $\Omega = \mu_{ac}E_c/\hbar$  and  $g\varepsilon = \mu_{ab}E_p/\hbar$  using the field strengths  $E_{c(p)} = \sqrt{I_{c(p)}/c\varepsilon_0}$  and be  $\Omega = 1.13 \times 10^{10} \text{ s}^{-1}$  and  $g\varepsilon = 4.4 \times 10^8 \text{ s}^{-1}$ , respectively ( $g = 1.3 \times 10^6 \text{ s}^{-1}$  and  $N = 27.7 \times 10^8$ ). These parameters meet the condition  $\Gamma_{ab} < \Omega$  for the strong atom-field coupling in the system.

At near-resonance interaction, when  $\Delta_c/d_0\Gamma_{ac} \approx 0.1$  at  $d_0 = 0.308$  and  $\Delta_c = 3 \times 10^7 \text{ s}^{-1}$ , the nonlinear coupling between the probe and pump fields is actually absent as it follows from Fig. 2. This is due to the fact that during the interaction the ground state  $|b\rangle$  is hardly depopulated ( $\sigma_{bb} \approx 1$ ) and in the absence of the atoms in states  $|a\rangle$  and  $|c\rangle$  the resulting polarization conditioned by transition  $|a\rangle \rightarrow |b\rangle$  is weak (see in Fig. 2a). In this case, the solutions of Eqs. (1) and (3) for the matrix element  $\sigma_{ba}$  can approximate one another with sufficient accuracy as a proof of validity of approximations used in the derivation of (3). Figure 2a shows the regime typical for the linear EIT effect in a three-level medium [29], or its non-linear analogue [30] at a significant increase of the pump intensity.

Quite different dynamics related to the nonlinear interaction of the fields may be expected when we chose the Raman interaction mode when  $\Delta_c > \Omega > d_0\Gamma_{ab}$ . This interaction mode is long-known [9, 10] and well studied, but it did not get a strong “scientific resonance” in terms of its prospects of practical use in modern optical technologies, as it happened with EIT. This mode is characterized by a set of curves for the matrix elements in Fig. 2b, obtained for parameters the same as in Fig. 2a but with greater detuning  $\Delta_c = 3 \times 10^{10} \text{ s}^{-1}$  and condition  $\Delta_c/d_0\Gamma_{ac} \approx 100$ . In this case the atomic state  $|b\rangle$  is effectively depopulated giving population mostly to state  $|c\rangle$ . This presupposes the emergence of a significant polarization in transition  $|a\rangle \rightarrow |b\rangle$ . It seems apparent if we compare the scale of values  $\sigma_{ba}$  in Figs. 2a and 2b (the same is true for the transition  $|a\rangle \rightarrow |c\rangle$ ). This fact leads to the establishment of a nonlinear energy transfer between modes of the probe and pump fields. This is the interaction mode we are going to use further in our analysis.

The weak coupling in the atom-field system  $\Gamma_{ab} > \Omega$  for both modes in Figs. 2a and 2b produces a significant discrepancy between solutions obtained from (1) and (3) as one may see in Fig. 2c at  $\Delta_c = 3 \times 10^7 \text{ s}^{-1}$ ,  $\Omega = 1.13 \times 10^8 \text{ s}^{-1}$ . In particular, this is due to a violation of the condition  $\Omega \gg \sigma_{ca}\chi_{ca}$  and the need to account for the effects of the local field for transition  $|a\rangle \rightarrow |c\rangle$ . This fact complicates the task and requires a direct nu-

merical simulation of the self-consistent problem (2) and (3) [31]. It makes further analysis of opportunities to obtain solitons, including spatial solitons, very troublesome because of major transformations of the matrix elements.

Now let us find the steady state solution for the density matrix element  $\sigma_{ba}$  of the probe transition in a form that depends only on the material parameters of the media and the characteristics of the optical fields considering various cases of atom-field interaction. In order to do this, we should solve Eqs. (3) in two steps. The first step is to define the polarization of the system at the lower levels  $\sigma_{cb}$  as based on the approximation of constant populations and atomic polarizations in the steady state, i.e.,  $\dot{\sigma}_{aa} = \dot{\sigma}_{bb} = \dot{\sigma}_{cc} = 0$  and  $\dot{\sigma}_{ba} = \dot{\sigma}_{ca} = \dot{\sigma}_{bc} = 0$ . At this point from Eqs. (3) we obtain an algebraic equation for the polarization  $\sigma_{bc}$ :

$$\Omega\chi g\varepsilon^* \sigma_{bc}^2 + i \left( \Gamma_1 g^2 |\varepsilon|^2 + \Gamma_2^* A \right) \sigma_{bc} + i g \varepsilon \Omega^* \Gamma_2^* = 0, \quad (4)$$

the roots of which are the following:

$$\sigma_{bc} = \frac{-i \left( \Gamma_1 g^2 |\varepsilon|^2 + \Gamma_2^* A \right) \pm \sqrt{D}}{2\Omega\chi g\varepsilon^*}, \quad (5)$$

where  $D = - \left( \Gamma_1 g^2 |\varepsilon|^2 + \Gamma_2^* A \right)^2 - 4i\chi g^2 |\Omega|^2 \Gamma_2^* |\varepsilon|^2$ ,  $A = |\Omega|^2 - i\Delta_3 (\Gamma_1 + i\chi)$ ,  $\chi \equiv \chi_{ba}$ .

Solutions (5) determine, in fact, the two branches of spin excitations that occur at the transition between levels  $|b\rangle$  and  $|c\rangle$  (see Fig. 1). The solution that contains the minus sign in (5) leads to a problem with the saturating nonlinearity  $\sigma_{bc} \approx 1/\varepsilon$  and is not considered in this paper. Expansion of the other solution, that is positive, in series of the pump field  $\varepsilon$  gives the following relationship:

$$\begin{aligned} \sigma_{bc} \approx & -\frac{g\Omega^*}{A}\varepsilon + \frac{g^3\Omega^*}{\Gamma_2^* A^2} \left( \Gamma_1 + i\frac{|\Omega|^2\chi}{A} \right) |\varepsilon|^2 \varepsilon \\ & - \frac{g^5\Omega^*}{(\Gamma_2^*)^2 A^3} \left( \Gamma_1^2 + \frac{3i|\Omega|^2\chi\Gamma_1}{A} - \frac{2\chi^2|\Omega|^4}{A^2} \right) |\varepsilon|^4 \varepsilon. \end{aligned} \quad (6)$$

Our second step is to use the equations for both  $\dot{\sigma}_{ca}$  and  $\dot{\sigma}_{bc}$  in (3) to write the atomic polarization from the probe transition:

$$\sigma_{ba} = \frac{\left( \Delta_3 + i\frac{g^2|\varepsilon|^2}{\Gamma_2^*} \right) \sigma_{bc} + i\frac{g\varepsilon\chi}{\Omega\Gamma_2^*} |\sigma_{bc}|^2 \left( \Delta_3 - i\frac{g^2|\varepsilon|^2}{\Gamma_2} \right)}{\Omega^* - \frac{g^2|\varepsilon|^2\chi^2}{\Omega|\Gamma_2|^2} |\sigma_{bc}|^2} \quad (7)$$

Now we substitute expansion (6) into (7) and perform the secondary expansion to get

$$\begin{aligned}
\sigma_{ba} \approx & \frac{g\Delta_3}{A}\varepsilon - i\frac{g^3}{\Gamma_2^*A} \left( 1 + i\Delta_3 \left( \frac{\Gamma_1}{A} + i\frac{\chi}{A^*} + i\frac{\chi|\Omega|^2}{A^2} \right) \right) |\varepsilon|^2 \varepsilon \\
& + g^5 \left( \frac{1}{(A\Gamma_2^*)^2} \left[ i \left( 1 - \frac{\chi\Delta_3}{A^*} \right) \left( \Gamma_1 + i\frac{\chi|\Omega|^2}{A} \right) - \frac{\Delta_3}{A} \left( \Gamma_1^2 - 2\frac{\chi^2|\Omega|^4}{A^2} + 3i\frac{\chi\Gamma_1|\Omega|^2}{A} \right) \right] \right. \\
& \left. - \frac{i\chi}{|A|^2|\Gamma_2|^2} \left( i + \frac{\Delta_3}{A^*} \left\{ \Gamma_1^* - i\frac{\chi|\Omega|^2}{A^*} \right\} - i\frac{\chi\Delta_3}{A} \right) \right) |\varepsilon|^4 \varepsilon.
\end{aligned} \tag{8}$$

In Fig. 2 solution (8) is represented by a thick solid line, which is in agreement with the solutions of (1) and (3) to a high degree of accuracy as a clear proof of the correctness of (8). Let us note that if solving Eqs. (3) in the EIT limit, when it can be assumed that  $\sigma_{ac} = 0$ , the expression for  $\sigma_{bc}$  contains only the first term in the right-hand side of (6) (see [29]). In its turn, Eq. (7) now becomes

$$\sigma_{ba} = \frac{\Delta_3\sigma_{bc}}{\Omega^*} = \frac{g\Delta_3}{A}\varepsilon \tag{9}$$

and determines the appearance of the phase modulation and the absorption (amplification) of the probe pulse in the atomic medium. We found that the appropriate solution for this linear mode (9) for  $\sigma_{ba}$  with sufficient accuracy coincides with the solutions of (1) and (3) in Fig. 2a. The later proves the validity of the theory and the limiting cases as well.

For further analysis we will focus on the situation shown in Fig. 2b and move on to the study of the spatial dynamics (in the plane perpendicular to the direction of propagation) of optical pulses in the hollow-core fiber filled with resonant atoms as shown in Fig. 1, and consider the possibility of obtaining a special kind of stable structures known as vortex solitons [3] of the probe field.

### III. VARIATIONAL APPROACH FOR STABLE VORTEX SOLITONS IN A THREE-LEVEL MEDIUM

In the Raman limit for the  $\Lambda$ -type interaction scheme (Fig. 1) after substituting (8) into the propagation equation (2), the self-consistent problem of spatial dynamics (2)-(3) is reduced to the well-known form of the Ginzburg-Landau equation (see [3]):

$$\begin{aligned}
\left( \frac{1}{c} \frac{\partial}{\partial t} + \frac{\partial}{\partial z} \right) \varepsilon - i\frac{D}{2} \left( \frac{\partial^2 \varepsilon}{\partial x^2} + \frac{\partial^2 \varepsilon}{\partial y^2} \right) \\
- i\gamma_2 |\varepsilon|^2 \varepsilon + i\gamma_4 |\varepsilon|^4 \varepsilon = -\alpha_I \varepsilon - \alpha_2 |\varepsilon|^2 \varepsilon - \alpha_4 |\varepsilon|^4 \varepsilon,
\end{aligned} \tag{10}$$

where the corresponding coefficients are the following:

$$\gamma_2 = \text{Im} \left\{ -\frac{g^4 N}{A\Gamma_2^* c} \left( 1 + i\Delta_3 \left\{ \frac{\Gamma_1}{A} + \frac{i\chi}{A^*} + i\frac{\chi|\Omega|^2}{A^2} \right\} \right) \right\}$$

is the cubic nonlinearity;

$$\begin{aligned}
\gamma_4 = \text{Im} \left\{ \frac{ig^6 N}{c} \left( \frac{1}{(A\Gamma_2^*)^2} \left[ i \left( 1 - \frac{\chi\Delta_3}{A^*} \right) \left( \Gamma_1 + i\frac{\chi|\Omega|^2}{A} \right) \right. \right. \right. \\
\left. \left. - \frac{\Delta_3}{A} \left( \Gamma_1^2 - 2\frac{\chi^2|\Omega|^4}{A^2} + 3i\frac{\chi\Gamma_1|\Omega|^2}{A} \right) \right] \right. \right. \\
\left. \left. - \frac{i\chi}{|A|^2|\Gamma_2|^2} \left( i + \frac{\Delta_3}{A^*} \left\{ \Gamma_1^* - i\frac{\chi|\Omega|^2}{A^*} \right\} - i\frac{\chi\Delta_3}{A} \right) \right) \right\}
\end{aligned}$$

is the quintic nonlinearity;

$$\alpha_I = \text{Im} \left\{ \frac{g^2 N \Delta_3}{Ac} \right\}$$

is the linear loss coefficient;

$$\alpha_2 = \text{Re} \left\{ \frac{g^4 N}{A\Gamma_2^* c} \left( 1 + i\Delta_3 \left\{ \frac{\Gamma_1}{A} + \frac{i\chi}{A^*} + i\frac{\chi|\Omega|^2}{A^2} \right\} \right) \right\}$$

is the cubic loss;

$$\begin{aligned}
\alpha_4 = \text{Re} \left\{ \frac{ig^6 N}{c} \left( \frac{1}{(A\Gamma_2^*)^2} \left[ i \left( 1 - \frac{\chi\Delta_3}{A^*} \right) \left( \Gamma_1 + i\frac{\chi|\Omega|^2}{A} \right) \right. \right. \right. \\
\left. \left. - \frac{\Delta_3}{A} \left( \Gamma_1^2 - 2\frac{\chi^2|\Omega|^4}{A^2} + 3i\frac{\chi\Gamma_1|\Omega|^2}{A} \right) \right] \right. \right. \\
\left. \left. - \frac{i\chi}{|A|^2|\Gamma_2|^2} \left( i + \frac{\Delta_3}{A^*} \left\{ \Gamma_1^* - i\frac{\chi|\Omega|^2}{A^*} \right\} - i\frac{\chi\Delta_3}{A} \right) \right) \right\}
\end{aligned}$$

is the quintic loss.

It is obvious that Eq. (10) is the result of a complicated nonlinear interaction between the probe field and the pump field which arises solely due to the presence of significant values of polarizations of the optical transitions in the Raman limit of the  $\Lambda$ -configuration [11]. Even though the locally acting field used in this theory does not produce new terms in Eq. (10) it, however, gives certain corrections to the picture of the nonlinear interaction (terms with  $\chi$ -factor) for the case of an optically dense medium. Let us note that in another limit of the  $\Lambda$ -configuration the near-resonance conditions, i.e.  $\Delta_b \ll \Gamma_{ab}$ , would simplify Eq. (10) by eliminating its nonlinear terms. The local field in this case would be insignificant as it can only lead to an additional phase modulation in the probe field [32].

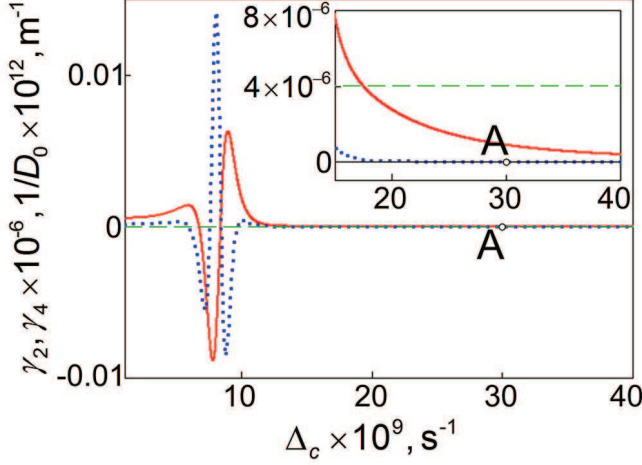


Figure 3. Frequency dependences of the third  $\gamma_2$  (red solid line) and fifth-order  $\gamma_4$  (blue dotted line) nonlinearities, and the backward diffraction (green dashed line). The inset shows the enlarged image of the region near the point A. The interaction parameters are the same as in Fig. 2(b).

In order to start the analysis of (10) we will first transform to the moving coordinate system  $T = t - z/c$  and perform the change of variables  $u = \varepsilon/\sqrt{|\varepsilon_{in}|^2}$ ,  $\xi = z/L_{df}$ ,  $X = x/a_0$ ,  $Y = y/a_0$ . Our second step is to define the following main characteristic lengths:  $L_{\gamma_2} = 1/(\gamma_2 |\varepsilon_{in}|^2)$  and  $L_{\gamma_4} = 1/(\gamma_4 |\varepsilon_{in}|^4)$  are the nonlinearities of the third and the fifth orders respectively;  $L_{\alpha I} = 1/\alpha_I$  describes the linear losses,  $L_{\alpha 2} = 1/(\alpha_2 |\varepsilon_{in}|^2)$  and  $L_{\alpha 4} = 1/(\alpha_4 |\varepsilon_{in}|^4)$  describe the nonlinear losses of the third and fifth orders;  $L_{df} = a_0^2/D$  is the diffraction length, where  $\varepsilon_{in}$  is the reduced amplitude of the beam at the entrance point. After multiplying both sides of (10) by  $L_{df}$  we finally get

$$i \frac{\partial U}{\partial \xi} + \frac{1}{2} \left( \frac{\partial^2 U}{\partial X^2} + \frac{\partial^2 U}{\partial Y^2} \right) + |U|^2 U - \nu |U|^4 U = Q, \quad (11)$$

where  $Q = i[-\delta U - \phi |U|^2 U - \mu |U|^4 U]$  is the dissipative part, for which we have the following notations  $U = uN$  and  $N^2 = L_{df}/L_{\gamma_2}$ , and the main characteristic parameters:  $\delta = L_{df}/L_{\alpha I}$ ,  $\phi = L_{\gamma_2}/L_{\alpha 2}$ ,  $\mu = L_{\gamma_2}^2/(L_{\alpha 4} L_{df})$ ,  $\nu = L_{\gamma_2}^2/(L_{\gamma_4} L_{df})$ .

For the formation of a conservative optical soliton the interaction parameters should be selected in such a way that the characteristic nonlinear and diffraction lengths were approximately comparable or multiples of each other [33]. This can be achieved near the region of strong transformations of the nonlinear coefficients by varying the detuning of the pump field as it is shown in Fig. 3. In particular, for the point  $\Delta_c^A$  the diffraction length should be only  $L_{df} = 1.61$  mm so for the positive nonlinearity, i.e.  $\gamma_2 > 0$ , we may expect focusing and formation of a stable spatial soliton. However, following the

concept of dissipative solitons, to maintain the energy of bright solitons at a constant level it would require interchanging between absorption and gain effects in different areas of the probe envelope, in particular, when these inequalities  $\delta > 0$ ,  $\phi < 0$ ,  $\mu > 0$  are to be met [34]. Figure 4 shows the typical dissipative parameters as functions of the pump field intensity  $I_c$  at a fixed detuning  $\Delta_c^A$  as in Fig. 3 near the gain threshold. Under conditions of diverse variation of the dissipative coefficients with increasing pump intensity we can select  $I_c$  for fixed  $\Delta_c^A$  (or vice versa) to satisfy the condition of dynamic equilibrium for nonlinear and dissipative processes.

Using the variational approach for the analysis of (11) we may determine the ranges of parameters for which stable spatial solitons can occur. Our particular interest is focused on an important class of dissipative spatial vortex solitons of the kind described in [3]:

$$U = A_0 A \left( \frac{r}{R_0 R} \right)^S \exp \left\{ -\frac{r^2}{2(R_0 R)^2} + i \left( C \frac{r^2}{R_0^2} + S\theta + \Psi \right) \right\}, \quad (12)$$

where  $r = \sqrt{X^2 + Y^2}$ ,  $\theta$  is the angle in spherical coordinates and  $A$ ,  $R$ ,  $C$ , and  $\Psi$  are the amplitude, the spatial width, the curvature of the wave front and the phase of the pulse, respectively. Parameter  $S$  determines the topological charge of the vortex soliton. In the special case of  $S = 1$  the normalization coefficients  $A_0$  and  $R_0$  can be expressed in terms of the full power normalization

$$P = \int_0^{2\pi} \int_0^\infty |U(r, \theta)|^2 r dr d\theta = (\pi S! A_0^2 R_0^2) A^2 R^2.$$

In the simplest case, when  $P = A^2 R^2$ , they are related as  $A_0 = 1/(R_0 \sqrt{\pi})$  and  $R_0 = 1$ .

In practice, the effects of diffusion in atomic ensembles would fill the dark center of an optical vortex with light (12) even with presence of a long-lasting shape in the form of a bright soliton propagating in such media [4]. For a self-maintained special crater-shaped vortex solitons (12) the system would require not only a balance of the nonlinear, diffraction and dissipation effects [34] but also some presence of the optical diffusion [35] or a complicated type of modulation of either the refractive index [36] or the absorption coefficient [3] or both. In particular, the static parameter of the linear absorption can be replaced with a space-dependent effective parameter  $\delta_{eff} = \delta - V r^2$ . It would describe introduction of an additional saturable absorber into the fiber filled with a cold gas. This is the case we consider further in this paper and assume  $V = -0.03$  everywhere below. A detailed analysis of the stability of vortex solitons in the linearization of the master equation written in a form more general than (10) and with the optical diffusion taken into account is given in [37].

Now we use the Euler-Lagrange equation for the axisymmetric vortex soliton and we get the system of equa-



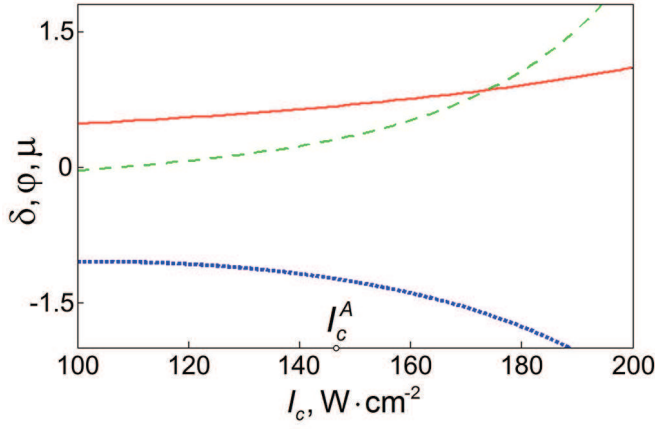


Figure 4. Parameters of the dissipative part of the non-dimensional Ginzburg-Landau equation  $\delta$  (solid red),  $\phi$  (dotted blue), and  $\mu$  (dashed green) as functions of the pump field intensity. The interaction parameters are the same as for point A in Fig. 3.

tions for the variable parameters:

$$\frac{dA}{d\xi} = -\frac{5\phi A^3}{16\pi} - \frac{8\mu A^5}{81\pi^2} + A(-\delta - C + VR^2), \quad (13a)$$

$$\frac{dR}{d\xi} = \frac{\phi A^2 R}{16\pi} + \frac{2\mu A^4 R}{81\pi^2} + CR + VR^3, \quad (13b)$$

$$\frac{dC}{d\xi} = -C^2 + \frac{1}{8R^4} - \frac{A^2}{16\pi R^2} + \frac{2\nu A^4}{81\pi^2 R^2}, \quad (13c)$$

$$\frac{d\Psi}{d\xi} = \frac{3A^2}{8\pi} - \frac{10\nu A^4}{81\pi^2} - \frac{1}{2R^2}. \quad (13d)$$

For a low frequency modulation ( $C^2 \cong 0$ ), as in [3], we come to the following system of equations, which simplifies the search for the fixed points for (13):

$$C = \frac{A^2(-81\pi\phi - 32A^2\mu)}{1296\pi^2} - \frac{162\pi^2 V}{A^2(81\pi - 32A^2\nu)}, \quad (14a)$$

$$R^2 = \frac{162\pi^2}{A^2(81\pi - 32A^2\nu)}, \quad (14b)$$

$$-\frac{5\phi A^3}{16\pi} - \frac{8\mu A^5}{81\pi^2} + A(-\delta - C + VR^2) = 0. \quad (14c)$$

Equations (14) give 16 steady state roots, among which only two correspond to the physical conditions on the energy and the width of the vortex soliton ( $A > 0$ ,  $R > 0$  and  $A, R \in \mathbb{R}$ ). Besides, only one of them would have the maximum value of  $A$  and negative frequency modulation ( $C < 0$ ) and be stable [3].

Figure 5 shows the parametric plane formed by the following parameters: the density of resonant atoms in the system  $\rho$  and the intensity of the pump field  $I_c$ . The region bounded by the dash-dot line refers to stability of

axisymmetric vortex solitons and arise for the selected physical solution of (14) [3]. This area was determined from the analysis of the eigenvalues of the Jacobi matrix for Eqs. (13), i.e., for condition  $\text{Re}(\lambda_j) < 0$ , where  $j = 1, 2, 3$  [38], and corresponds to the point of a stable focus.

Direct numerical simulations of Eq. (11) with variation of parameters for the function of the form (12) and taking into account the initial angular perturbation for  $R$  and  $C$  [39] show that the area of stable solutions obtained from simplified Eqs. (14) is very approximate. At the same time the true stability region I (in Fig. 5) is much smaller. The region of stability obtained using the variation approximation appears to have a “fine” structure in the form of separate zones for solitons with modified shapes as well as zone IV, where the optical vortices are damped.

In particular, in the area II in Fig. 5 (parameters as in Eq. (11):  $\nu = 0.1653$ ,  $\delta = 0.6819$ ,  $\phi = -1.1998$ ,  $\mu = 0.2432$  at  $\rho = 9.85 \times 10^{21} \text{ m}^{-3}$  and  $I_c = 146.2 \text{ W}\cdot\text{cm}^{-2}$  for point B) we find a spontaneous transition of an axisymmetric vortex into a single-humped asymmetric stable vortex soliton, presented in image B in Fig. 6. Bifurcations of this type are described in [3]. Region III in Fig. 5 (parameters as in Eq. (11):  $\nu = 0.2519$ ,  $\delta = 0.7158$ ,  $\phi = -1.2576$ ,  $\mu = 0.3169$  at  $\rho = 9.85 \times 10^{21} \text{ m}^{-3}$ ,  $I_c = 152 \text{ W}\cdot\text{cm}^{-2}$  for point C) is characterized by a high sensitivity of the system to initial perturbations. As these perturbations are developing the vortex soliton spontaneously loses its topological charge and transforms into a new stable state with  $S = 0$  (see image C in Fig. 6).

In area V the account for angular perturbation in Eq. (12) leads to destruction of vortex solitons and emergence of nonstationary localized structures in their place, which, however, do not damp but demonstrate some ongoing evolution [40]. At point D the field parameters in Eq. (11) take values  $\nu = 0.1043$ ,  $\delta = 0.674$ ,  $\phi = -1.14$ ,  $\mu = 0.1551$  at  $\rho = 9.6 \times 10^{21} \text{ m}^{-3}$  and  $I_c = 143.3 \text{ W}\cdot\text{cm}^{-2}$ . Here the axisymmetric vortex soliton transforms in a multi-hump structure rotating along its propagation path in the fiber as it is shown in image D in Fig. 6. It is also possible to observe a specific double-hump soliton [37] in image D' in Fig. 6. This structure occurs when  $\nu = 0.1297$ ,  $\delta = 0.6633$ ,  $\phi = -1.1848$ ,  $\mu = 0.228$  at  $\rho = 9.925 \times 10^{21} \text{ m}^{-3}$  and  $I_c = 143.3 \text{ W}\cdot\text{cm}^{-2}$ . In area IV we notice the loss of stability and complete damping of vortex solitons.

Let us note that point A (with the same set of parameters as in Fig. 3) is indeed found in the area of stability, calculated using both the variation approach and direct simulations, which is in agreement with the qualitative analysis of Eq. (11). Thus, formation of vortex solitons in our medium would require the initial spatial width and the curvature of the wave front of the light pulse in the form of Eq. (12) be  $r_R = 19 \mu\text{m}$  and  $C_R = -3.7 \times 10^6 \text{ m}^{-2}$  respectively. The dimensionless parameters are, therefore,  $A = 5.75$ ,  $R = 0.95$ , and  $C = -0.0015$ . The values calculated for Eq. (11) for point A in Fig. 5 are

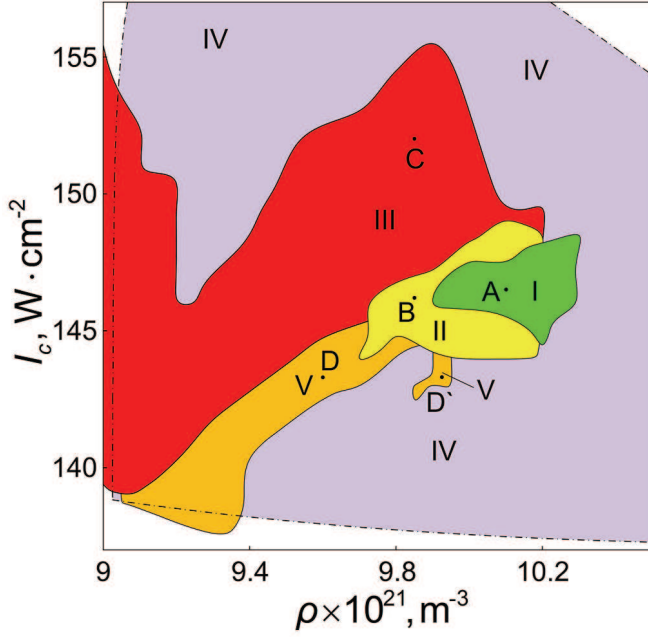


Figure 5. Parametric plane (the intensity of the pump field  $I_c$  vs the dopant density  $\rho$ ). The dash-dot line margins the area of stability for an axisymmetric vortex soliton obtained by the variation technique. The highlighted areas are obtained by direct numerical simulations and correspond to: green - axisymmetric vortex solitons, yellow - single-peak vortex solitons, red - irrotational solitons, orange - unsteady localized structures, purple - unstable structures. The interaction parameters correspond to Fig. 4.

$\nu = 0.1899$ ,  $\delta = 0.675$ ,  $\phi = -1.2375$ , and  $\mu = 0.3075$ . The soliton regime of such a structure is achieved within the characteristic length of  $L_{ST} = 4$  cm while the rotation period of the vortex wave front in this regime is  $T_V = 1.45$  cm (see image A in Fig. 6).

Figure 7 shows the region of stability for vortex solitons in the plane  $(I_c, V)$  at  $\rho = 1.015 \times 10^{22} \text{ m}^{-3}$ . The area of stability obtained by the variational approach extends to both the positive and negative areas of parameter  $V$ . The numerical simulation gives a narrower area and demonstrates that stable dissipative vortices can exist only for negative values of  $V$ .

The fundamental point in this problem is consideration of the local field effects. Indeed, if  $\chi = 0$ , that is, without taking them into account, the region of stability is not simply transformed, but it completely transcends the parametric areas shown in Fig. 4. In this case, all the solutions obtained for the vortex solitons become unstable. Thus, the strategy of the possible experiment should change dramatically with the local value of the acting field in the medium.

Further analysis and evaluation of the other stability regions for the vortex solitons require solution of the full nonlinear system (13) as well as an expanded multi-dimensional numerical experiment within the domain of the system's parameters.

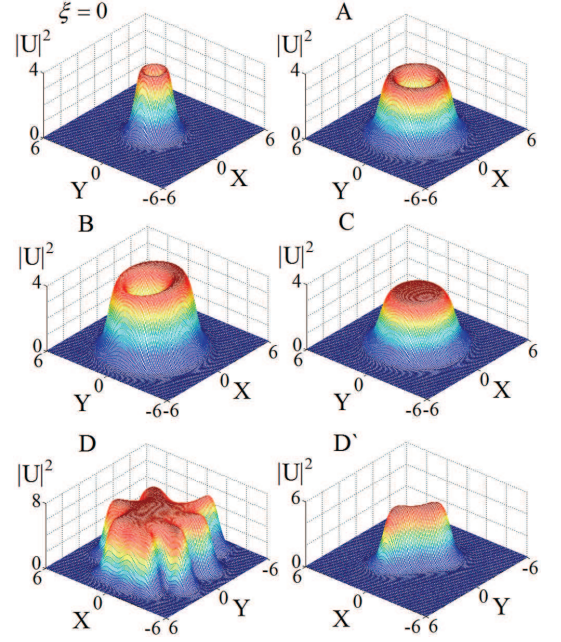


Figure 6. Results of direct numerical simulations of Eq. (11), i.e. spatial profiles in  $(X, Y)$ -plane of optical beams at the entrance  $\xi = 0$  and after traveling the distance of  $\xi = 100000$  in the gas-filled fiber in the presence of azimuthal perturbations. The letter in the upper left corner of each image corresponds to a point in the parameter plane in Fig. 5, the coordinates of which were used to calculate the parameters of the Eq. (11).

#### IV. STABILITY STRESS TESTING OF OPTICAL VORTICES UNDER PERTURBATIONS OF SYSTEM'S BASIC PARAMETERS

Let us consider the evolution of an optical vortex soliton (12) in terms of natural fluctuations or/and additional modulations of the optical fields and the atomic medium in the core of the fiber. Such perturbations may be associated with variations of the pump field intensity  $I_c(\xi, X, Y) = I_c^{\text{det}} + \zeta_I(\xi, X, Y)$  and the atomic density  $\rho(\xi, X, Y) = \rho^{\text{det}} + \zeta_\rho(\xi, X, Y)$ , where  $I_c^{\text{det}}$  and  $\rho^{\text{det}}$  describe the deterministic part. Parameters  $\zeta_I(\xi, X, Y)$  and  $\zeta_\rho(\xi, X, Y)$  are presented by three-dimensional matrices of fluctuations or periodic spatial modulation of the corresponding functions. Random perturbations of the intensity  $\zeta_I^{\text{rnd}}(\xi, X, Y)$  we describe as the Gaussian white noise. The density fluctuations in a Bose gas below the critical temperature at transformation to the dimensional parameters have a spatial correlation function of the form

$$\langle \zeta_\rho^{\text{rnd}}(r_1) \zeta_\rho^{\text{rnd}}(r_2) \rangle = \rho_0 (\delta(r_1 - r_2) + \nu_n(r_{\text{rnd}})), \quad (15)$$

where

$$r_i = (z_i, x_i, y_i),$$

$$\nu_n(r_{\text{rnd}}) = \frac{m_a k_B T \rho_b}{\pi \rho_0 \hbar^2 r_{\text{rnd}}} + \frac{3 m_0^2 k_B^2 T^2}{4 \pi^2 \rho_0 \hbar^4 r_{\text{rnd}}^2}.$$

In our numerical simulations we used the three characteristic spatial scales, i.e., the sampling interval of



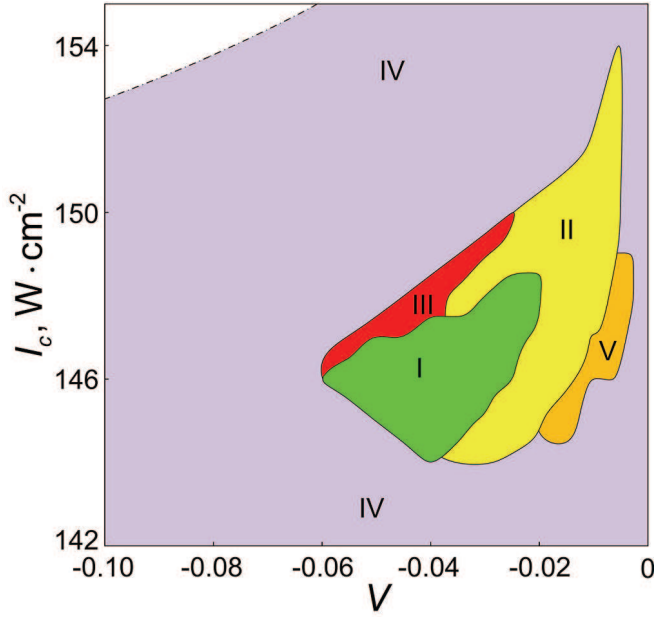


Figure 7. Parametric plane (the intensity of the pump field  $I_c$  vs. the optical trapping parameter  $V$ ). Interaction parameters and filling colours are the same as in Fig. 5.

$\xi_{st} = 0.0011$ , the characteristic length of density variation (physical step) of  $\xi_{rnd} = 0.0068$  (equivalent to  $r_{rnd} = 11 \mu\text{m}$ ) and  $\xi_{var} = 0.07$  for the characteristic distance at which the mean value of the noise becomes zero. The selected physical step is so great that  $\nu_n(r_{rnd})/\rho_0 \approx 0.4\%$ , so the second term in the right-hand side of Eq. (15) is neglected and we can model the density fluctuations using the white noise and spatial splines (Fig. 8a,b) for the convenience of calculations at the intermediate points.

The periodic perturbations of the pump field intensity  $\zeta_I^{\text{reg}}(\xi)$  and the atomic density  $\zeta_\rho^{\text{reg}}(\xi)$  with the amplitudes  $\zeta_{I_0}^{\text{reg}}$  and  $\zeta_{\rho_0}^{\text{reg}}$  are assumed to be effective only along axis  $z$ :  $\zeta_I^{\text{reg}}(\xi) = \zeta_{I_0}^{\text{reg}} \sin(2\pi\xi/L_I + \varphi_I)$  and  $\zeta_\rho^{\text{reg}}(\xi) = \zeta_{\rho_0}^{\text{reg}} \sin(2\pi\xi/L_\rho + \varphi_\rho)$  with the specified spatial periods  $L_I$ ,  $L_\rho$  and random initial phases  $\varphi_{I(\rho)}$ . The pulsations of the pump intensity can have two sources: the artificial modulation at the output of the pump laser or the intensity oscillations occurring in the pump depletion and gain saturation [41]. The periodic modulation of the density can be caused by an external mechanical action entailing excitation of acoustic waves in the system.

The specificity of our problem lies in the possibility of studying the overall picture of the development of perturbations of each GLE parameter and their impact on the dynamics of the soliton based on the perturbations of the basic parameters describing the media and the control fields. Quantitatively, this may be reflected by the values of the noise strength  $D_n = z_{var}(\delta n)^2$  for the GLE coefficients ( $\gamma_2, \gamma_4, \alpha_I, \alpha_2, \alpha_4$ ) with their mean-square deviations, calculated based on the presence of random perturbations in the system  $\varepsilon_I = \sigma_I/I_c^{\text{det}}$  and  $\varepsilon_\rho = \sigma_\rho/\rho^{\text{det}}$ ,

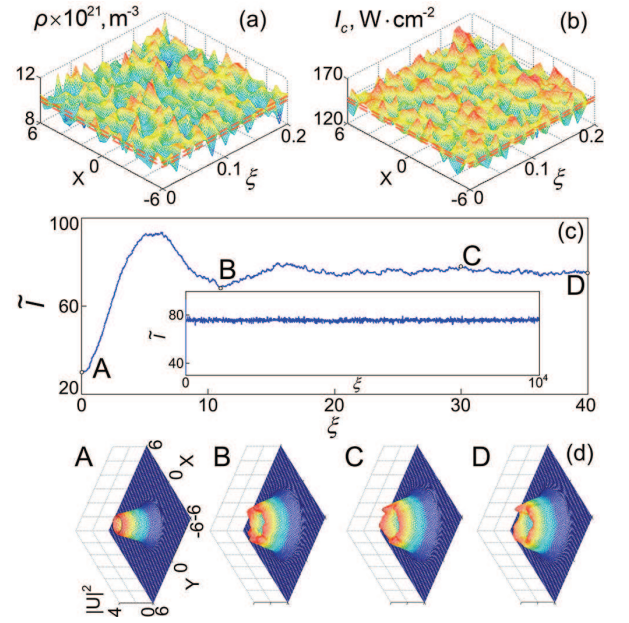


Figure 8. The model of the statistical stability for the axisymmetric vortex solitons with fluctuations of the atomic density  $\rho$  (a), the intensity of the pump field  $I_c$  (b). The range of the fluctuating quantities between the red lines corresponds to the stability area in Fig. 5. The temporal dynamics of the reduced power  $\tilde{I}$  of the soliton is shown in image (c), the profiles of the wave packet in image (d). The letter at the upper left corner of each image corresponds to the time in image (c).

where  $\sigma_I$  and  $\sigma_\rho$  are the mean-square deviations of variables, and  $z_{var} = \xi_{var} L_{df}$ . The possibility in our numerical simulation of collective impacts of noise + periodic modulation of the basic parameters completes the picture of the full-scale stress testing in the propagation regime of spatially localized structures.

To study the effect of perturbations on the vortex dynamics we performed a series of numerical experiments for different values of  $\sigma_I$  and  $\sigma_\rho$  and the control parameters  $I_c^{\text{det}}$  and  $\rho^{\text{det}}$ . As an indirect criterium of stability we assume the statistical stability of the reduced power

$$\tilde{I} = \int_0^{2\pi} \int_0^\infty |U(r, \theta)|^2 r dr d\theta$$

shown in Figs. 8-10 under perturbations  $\zeta_I(\xi, X, Y)$  and  $\zeta_\rho(\xi, X, Y)$ , and then we restore and analyze numerically the shape of the soliton in the desired point on axis  $\xi$ .

The longitudinal perturbations give rise to the inert properties of the soliton, i.e., the presence of noise, in which the phase trajectories  $\rho(\xi, X, Y)$ ,  $I_c(\xi, X, Y)$  never leave the stability region I in Fig. 5, does not cause dramatic consequences. Beyond the stability area the dynamics of a vortex is determined by the retardation effects in changing its shape compared to the rapid changes in GLE parameters initiated by the noise. Figure 8 shows the case of the maximum-allowable noise parameters  $\varepsilon_I^{\text{cr}} = 5.1\%$  and  $\varepsilon_\rho^{\text{cr}} = 7.4\%$  ( $I_c^{\text{det}} = 146.5 \text{ W}\cdot\text{cm}^{-2}$

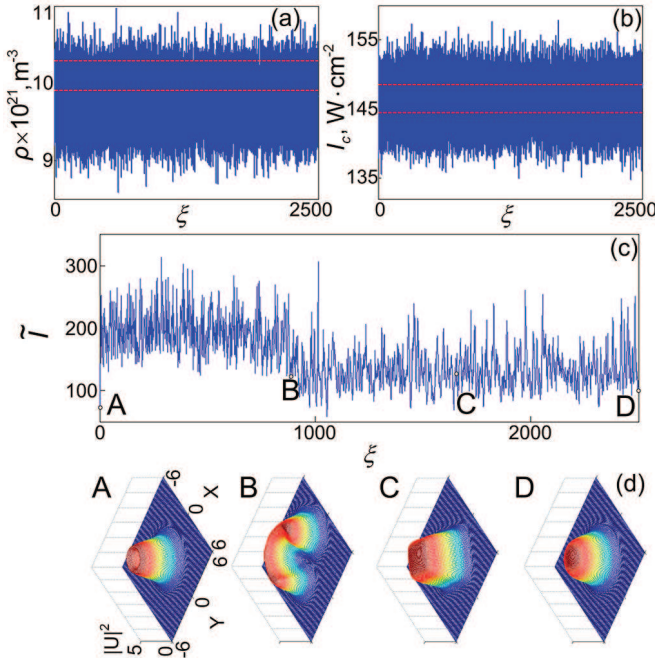


Figure 9. The model of the “breathing” state as a result of migration of the soliton solutions between regions III and V in Fig. 5 in presence of fluctuations (a) the atomic density matrix  $\rho$  and (b) the pump intensity  $I_c$ . Image (c) shows the temporal dynamics of  $\bar{I}$ ; corresponding to different time profiles of the probe wave packet in image (d).

and  $\rho^{\text{det}} = 10.1 \times 10^{21} \text{ m}^{-3}$  correspond to point A in Fig. 5) for the vortex soliton which preserves its shape over long distances  $z = 16.1 \text{ m}$  at  $\xi = 10000$  for values of the noise strength  $D_\mu = 3.2 \times 10^{-3}$ ,  $D_\nu = 1.1 \times 10^{-3}$ ,  $D_\delta = 1.66 \times 10^{-4}$ ,  $D_\phi = 1.1 \times 10^{-3}$ , see the inset in Fig. 8. The presence of the transverse perturbations in plane  $xOy$  leads to the noise-induced distortion of the wave packet profile in Fig. 8c but has almost no effect on its stability.

The continuous noise parameters in Eq. (11) for a point  $I_c^{\text{det}} = 146 \text{ W} \cdot \text{cm}^{-2}$  and  $\rho^{\text{det}} = 9.77 \times 10^{21} \text{ m}^{-3}$  from the transition area II in Fig. 5 can initiate reduction of topology and a jump transition of vortex solitons in a “breathing” mode with constant interconversion between the fundamental soliton and oscillating polygonal structure as in Fig. 9. This evolution is the result of walks the optical structure performs between areas III and V in Fig. 5 for values of noise strength  $D_\mu = 1.8 \times 10^{-3}$ ,  $D_\nu = 7.23 \times 10^{-4}$ ,  $D_\delta = 1.2 \times 10^{-4}$ ,  $D_\phi = 7.4 \times 10^{-4}$  which correspond to the perturbations  $\varepsilon_I = 1.92\%$  and  $\varepsilon_\rho = 2.87\%$  at  $\xi_{\text{rnd}} = 0.05$ . In transition of a soliton to the vortex-free mode one may observe formation of crescent-shaped optical structure as shown in Fig. 9d. In further rising of  $\sigma_I$  and  $\sigma_\rho$  there comes a transition into an unstable mode and decay, which is associated with a disproportionate increase in the noise intensity for various GLE coefficients. In this model the fifth-order nonlinear absorption coefficient  $\mu$  has a more rapid increase

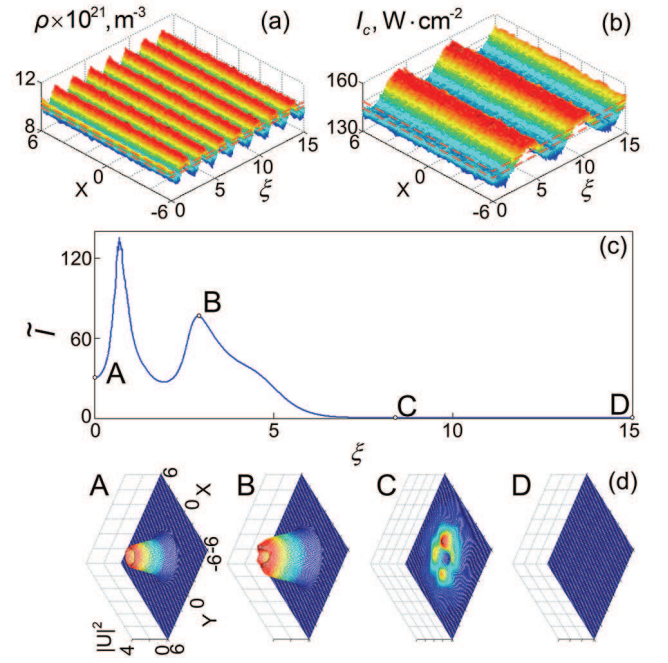


Figure 10. Model as a result of the loss of stability (a,b) periodic modulation of control parameters in the presence of a low-intensity noise. Image (c) shows the temporal dynamics of  $\bar{I}$ ; corresponding to different time profiles of the probe wave packet in image (d).

in the noise level and brings the soliton to zone IV in Fig. 5 and destroys it there.

The destructive effect are also caused by a weak periodic modulation of control parameters in the presence of a low intensity noise in Fig. 10, which collectively lead to fast violations of dynamic equilibrium in the system and damping of the soliton at scales of the order of  $\xi = 8$ . The simulation parameters correspond to  $\zeta_{I_0}^{\text{reg}} = 7.5 \text{ W/cm}^2$ ,  $\varphi_I = -2.51$  and  $\zeta_{\rho_0}^{\text{reg}} = 0.75 \times 10^{21} \text{ m}^{-3}$ ,  $\varphi_\rho = 2.76$ ,  $L_I = 6$ ,  $L_\rho = 2$  at constant values of  $I_c^{\text{det}}$  and  $\rho^{\text{det}}$  as for point A in Fig. 5. The scale of density fluctuations in Fig. 10 is 3.2 mm that given the expression for the speed of sound in a Bose gas  $c_{sn} = (\hbar/m_0)\sqrt{4\pi a_a \rho}$  [42] corresponds to the frequency 1 Hz of the sound wave with its speed 3.2 mm/s, where  $m_0$  is the mass of a single atom and  $a_a$  is the scattering amplitude. In the process of damping of the vortex soliton the system shows the rapid development of angular perturbations leading to the emergence of two or multihump unstable localized structures. This behavior is associated with a large spatial scale of the simulated pulsing perturbations which keep the vortex in violation of the conditions of dynamic equilibrium for a long time.

The well-known estimates for the modern laser systems that are compatible with the telecommunication channels determine the maximum allowable noise level of the output intensity to be not higher than 1%. This estimation by a large margin falls within the considered theory of stability of vortex solitons. Particle number fluctuations

of a Bose gas in the range of  $T < T_{cr}$  have the temperature dependence [43]

$$\sigma_N^2 = \frac{\pi^2}{6\zeta(3)} N \left( \frac{T}{T_{cr}} \right)^3.$$

This equation provides a simple expression for estimating the maximum density fluctuation in BEC  $\varepsilon_\rho = \pi(6\zeta(3)N)^{-1/2} \cong 1.17N^{-1/2}$  under condition that  $T = T_{cr}$ . For  $N = 3 \times 10^4$  and  $\omega_0 = 50$  kHz the critical temperature is 72  $\mu$ K. The maximum density fluctuation in such a system is 0.68%, which is 10 times as low as the maximum allowed atomic noise calculated for soliton mode in Fig. 8. This fact makes it evident to observe the vortex soliton regime at a temperature below the critical temperature for BEC.

In Figs. 8-10 we also consider the fluctuations of diffraction parameter emerging in the cross-section with the spatial scale within the range of the field's wavelength. This requirement arises from the fact that the present fluctuations of the gas density effectively modulate the refractive index of the medium. They also create a random phase delay, which with the finite width of the emission line produce the wavelength noise parameter. However, the simulation shows a statistically stable picture with the presence of local perturbations of soliton shapes even at 10% deviations of  $\lambda$ . This is similar to the initial angular perturbations of the vortex shapes which are smoothed after elimination of the noise.

## V. CONCLUSION

This study may give some ideas that could be useful for development of optical communication channels using vortex solitons in hollow-core fibers filled with a cold atomic gas. With the given fiber's parameters and the proper intensity of the probe field one may simultaneously tune the intensity and frequency of cw pump field to provide the conditions for the soliton propagation regime of vortex structures in the optical system. Because of the nonlinear contribution from the local field effects to development of competitive optical processes in a dense atomic medium the NDD corrections should

adjust the values of the control parameters for which we expect appearance of the solitons. For the parameters used in direct simulations the maximum fluctuations of the pump intensity and the probe wavelength that allow the soliton regime impose minor restrictions on the stability of the pump laser power and the probe laser frequency. The estimates for the atomic fluctuations gives an opportunity to observe the optical vortex solitons in the core-filling gas of the fiber for temperatures smaller than the critical temperature for BEC. The large-scale perturbations in the development of acoustic waves and the modulations of the pump field in the fiber can quickly destroy the soliton propagation regime even if they are of small amplitude.

For long-term maintenance of the BEC state in the information channel it is possible to use fine fibers filled with BEC atoms with a core diameter of the order of one micron or less [44]. Longer lifetimes of a coherent state in such a system are due to the geometry of the fiber and, in addition, the effect of channeling of atoms at creating the surface light wave along its core, causing the atoms to lose their energy effectively. The estimates given in [44] show that for the density  $10^{15} \text{ cm}^{-3}$  the temperature inside the fiber drops down to  $1.5 \times 10^{-5} \text{ K}$ .

However, such an elongated BEC must be assumed as a 1D gas so it is necessary to use some different relations for the fluctuations [45] at which observation of the vortex solitons is possible. Except it, the use of thin hollow-core fibers for optical communication due to the need to create localized optical structures at nanoscale, but in solving such a problem transition to the Maxwell equations for continuous media is impossible, and the effects of the near-field will play a crucial role.

## VI. ACKNOWLEDGMENTS

This work was supported by Russian Foundation for Basic Research Grant No. 12-02-31573 mol\_a and the Ministry of Education and Science of the Russian Federation under the program "Scientific and scientific-pedagogical potential of Russia for innovation" (Project No. 14.132.21.1397).

- 
- [1] Y. S. Kivshar and G. Agrawal, *Optical Solitons: From Fibers to Photonic Crystals* (Academic Press, 2003).
  - [2] N. N. Rozanov, *Dissipativniye opticheskie solitony. Ot micro- k nano- i atto-* (FIZMATLIT, 2012).
  - [3] V. Skarka, N. B. Aleksić, H. Leblond, B. A. Malomed, and D. Mihalache, *Phys. Rev. Lett.* **105**, 213901 (2010).
  - [4] R. Pugatch, M. Shuker, O. Firstenberg, A. Ron, and N. Davidson, *Phys. Rev. Lett.* **98**, 203601 (2007).
  - [5] A. Smith and D. Armstrong, *Opt. Express* **11**, 868 (2003).
  - [6] K. Bezuhanov, A. Dreischuh, G. G. Paulus, M. G. Schätzel, and H. Walther, *Opt. Lett.* **29**, 1942 (2004).
  - [7] P. Genevet, S. Barland, M. Giudici, and J. R. Tredicce, *Phys. Rev. Lett.* **104**, 223902 (2010).
  - [8] A. Prokhorov, M. Gubin, A. Leksins, M. Gladush, A. Alodjants, and S. Arakelian, *Journal of Experimental and Theoretical Physics* **115**, 1 (2012).
  - [9] A. V. Gorbach, D. V. Skryabin, and C. N. Harvey, *Phys. Rev. A* **77**, 063810 (2008).
  - [10] B. J. Herman, J. H. Eberly, and M. G. Raymer, *Phys. Rev. A* **39**, 3447 (1989).

- [11] A. V. Gorshkov, A. André, M. D. Lukin, and A. S. Sørensen, *Phys. Rev. A* **76**, 033805 (2007).
- [12] M. Bajcsy, S. Hofferberth, T. Peyronel, V. Balic, Q. Liang, A. S. Zibrov, V. Vuletic, and M. D. Lukin, *Phys. Rev. A* **83**, 063830 (2011).
- [13] A. B. Fedotov, S. O. Konorov, V. P. Mitrokhin, E. E. Serebryannikov, and A. M. Zheltikov, *Phys. Rev. A* **70**, 045802 (2004).
- [14] E. E. Serebryannikov, A. M. Zheltikov, S. Köhler, N. Ishii, C. Y. Teisset, T. Fuji, F. Krausz, and A. Baltuška, *Phys. Rev. E* **73**, 066617 (2006).
- [15] R.-J. Essiambre, G. J. Foschini, G. Kramer, and P. J. Winzer, *Phys. Rev. Lett.* **101**, 163901 (2008).
- [16] F. A. Hopf, C. M. Bowden, and W. H. Louisell, *Phys. Rev. A* **29**, 2591 (1984).
- [17] D. Kuznetsov, V. Roerich, and M. Gladush, *Journal of Experimental and Theoretical Physics* **113**, 647 (2011).
- [18] R. A. Vlasov and A. M. Lemeza, *Phys. Rev. A* **84**, 023828 (2011).
- [19] M. E. Crenshaw, *Phys. Rev. A* **78**, 053827 (2008).
- [20] L. F. Mollenauer, P. V. Mamyshev, and M. J. Neubelt, *Opt. Lett.* **21**, 1724 (1996).
- [21] M. Chertkov, I. Gabitov, P. M. Lushnikov, J. Moeser, and Z. Toroczkai, *J. Opt. Soc. Am. B* **19**, 2538 (2002).
- [22] R. Graham and T. Tél, *Phys. Rev. A* **42**, 4661 (1990).
- [23] C. Cartes, O. Descalzi, and H. R. Brand, *Phys. Rev. E* **85**, 015205 (2012).
- [24] A. Einstein, *Annalen der Physik* **322**, 549 (1905).
- [25] M. von Smoluchowski, *Annalen der Physik* **326**, 756 (1906).
- [26] S. Giorgini, L. P. Pitaevskii, and S. Stringari, *Phys. Rev. Lett.* **80**, 5040 (1998).
- [27] V. V. Kocharovsky, V. V. Kocharovsky, and M. O. Scully, *Phys. Rev. A* **61**, 053606 (2000).
- [28] V. Bagnato, D. E. Pritchard, and D. Kleppner, *Phys. Rev. A* **35**, 4354 (1987).
- [29] M. Fleischhauer and M. D. Lukin, *Phys. Rev. A* **65**, 022314 (2002).
- [30] I. Vadeiko, A. V. Prokhorov, A. V. Rybin, and S. M. Arakelyan, *Phys. Rev. A* **72**, 013804 (2005).
- [31] G. Demeter, D. Dzsojtan, and G. P. Djotyan, *Phys. Rev. A* **76**, 023827 (2007).
- [32] R. Fleischhaker, T. N. Dey, and J. Evers, *Phys. Rev. A* **82**, 013815 (2010).
- [33] G. Agrawal, *Applications of Nonlinear Fiber Optics (Optics and Photonics)* (Academic Press, 2001).
- [34] N. Akhmediev and A. Ankiewicz, *Dissipative Solitons: From Optics to Biology and Medicine (Lecture Notes in Physics)* (Springer, 2008).
- [35] D. Mihalache, D. Mazilu, F. Lederer, H. Leblond, and B. A. Malomed, *Phys. Rev. A* **76**, 045803 (2007).
- [36] D. Mihalache, D. Mazilu, V. Skarka, B. A. Malomed, H. Leblond, N. B. Aleksić, and F. Lederer, *Phys. Rev. A* **82**, 023813 (2010).
- [37] S. Fedorov, N. Rosanov, A. Shatsev, N. Veretenov, and A. Vladimirov, *Quantum Electronics, IEEE Journal of* **39**, 197 (2003).
- [38] L. Pontryagin, *Obyknovennye differentsialnye uravneniya* (Nauka, 1974).
- [39] V. Skarka, N. B. Aleksić, M. Derbazi, and V. I. Berezhiani, *Phys. Rev. B* **81**, 035202 (2010).
- [40] N. Rozanov, S. Fedorov, and A. Shatsev, *Optics and Spectroscopy* **95**, 843 (2003).
- [41] R. V. Johnson and J. H. Marburger, *Phys. Rev. A* **4**, 1175 (1971).
- [42] L. P. Pitaevskii and E. M. Lifshitz, *Statistical Physics, Part 2: Volume 9 (Course of Theoretical Physics Vol. 9)* (Butterworth-Heinemann, 1980).
- [43] H. D. Politzer, *Phys. Rev. A* **54**, 1050 (1996).
- [44] V. Balykin, D. Laryushin, M. Subbotin, and V. Letokhov, *Journal of Experimental and Theoretical Physics Letters* **63**, 802 (1995).
- [45] D. S. Petrov, G. Shlyapnikov, and J. T. M. Walraven, *Phys. Rev. Lett.* **85**, 3745 (2000).